Article

A Detailed Parametric Analysis of a Solar-Powered Cogeneration System for Electricity and Hydrogen Production

Panagiotis Lykas [ID], Nikolaos Georgousis, Angeliki Kitsopoulou, Dimitrios N. Korres, Evangelos Bellos *[ID] and Christos Tzivanidis [ID]

Thermal Department, School of Mechanical Engineering, National Technical University of Athens, Heroon Polytechniou 9, 15780 Athens, Greece
*   Correspondence: bellose@central.ntua.gr

Abstract: Hydrogen has received increased attention in the last decades as a green energy carrier and a promising future fuel. The integration of hydrogen, as well as the development of cogeneration plants, makes the energy sector more eco-friendly, and sustainable. The aim of this paper is the investigation of a solar-fed cogeneration system that can produce power and compressed green hydrogen. The examined unit contains a parabolic trough collector solar field, a thermal energy storage tank, an organic Rankine cycle, and a proton exchange membrane water electrolyzer. The installation also includes a hydrogen storage tank and a hydrogen compressor. The unit is analyzed parametrically in terms of thermodynamic performance and economic viability in steady-state conditions with a developed and accurate model. Taking into account the final results, the overall energy efficiency is calculated at 14.03%, the exergy efficiency at 14.94%, and the hydrogen production rate at 0.205 kg/h. Finally, the payback period and the net present value are determined at 9 years and 122 k€, respectively.

Keywords: solar system; cogeneration; ORC; green hydrogen; H_2O electrolysis; parametric analysis

1. Introduction

Over the last years, increasing energy demand and the domination of fossil fuels in the energy sector have led to serious environmental problems, and high greenhouse gas emissions [1]. So, both international organizations and governments around the globe have promoted environmentally friendly, and sustainable energy policies, which are based on the incorporation of renewable energy sources, as well as energy savings, efficiency enhancement, and the elimination of fossil fuel combustion [2]. Among renewable energy sources, solar energy is a clean energy source that can fulfill the global energy demand. Solar energy can be directly converted into electricity using photovoltaic (PV) devices and/or stored as solar heat energy [3]. In the direction of high energy efficiency and the reduction of carbon emissions, other solutions have also been proposed including the development of cogeneration, and multigeneration systems [4], as well as the increasing growth of alternative fuels such as green hydrogen [5]. These technologies can be incorporated into the energy sector to achieve sustainable development goals.

From the existing developed devices that exploit renewable energy sources, solar thermal collectors are the most promising technology to produce useful heat that achieves high energy performance and low financial cost. These systems can be utilized in both small-scale (space heating, domestic hot water) and large-scale applications (drying units, solar power plants) [6]. The most well-established and commercially available technology in this field is parabolic trough collectors (PTC). These collectors are made up of a linear parabolic reflector that concentrates solar irradiation and a tubular receiver. They operate at temperature values up to 400 °C using, most of the time, thermal oils as heat transfer fluids, and at higher temperature levels using molten salts. PTC and other concentrating collectors

are utilized to drive power cycles such as the Organic Rankine Cycle (ORC) [7]. In the ORC, an organic substance with a lower boiling point is utilized, while a low-temperature heat source is exploited, which comes from solar energy, geothermal energy, biomass, or waste heat [8].

A solar-fueled ORC configuration coupled to a PTC solar field with both warm and cold thermal energy storage tanks was examined in the literature by Yu et al. [9]. The recuperative ORC with toluene, which performed better than the other working media, achieved an overall efficiency, that increased by 24.8% compared to another published study. For the case of the supercritical ORC, both thermal and overall system efficiency were enhanced by 11.3% and 10.8%, respectively, compared to the corresponding sub-critical ORC. Moreover, another study [10] investigated a geothermal-based ORC energy system. The total energetic and exergetic efficiency was determined at 11.24% and 39.03%, respectively. Additionally, the incorporation of the recuperator improved both the energy and exergy efficiency by 15%. Furthermore, Bellos and Tzivanidis [11] analyzed an ORC plant powered by low-temperature waste heat and solar energy which was absorbed by PTCs. When toluene was utilized as the working medium, the overall energy efficiency reached the value of 19.7%. On the other hand, according to the literature, researchers have investigated energy plants based on ORC that produce more than one useful output, apart from electricity. Carraro et al. [12] studied a micro-cogeneration installation, which produced electricity and domestic hot water. The plant, which could be incorporated into microgrids, contained a biomass boiler and an ORC unit. Therminol SP was used in the heating circuit. So, the maximum value of the ORC electrical efficiency was found at 7.3%, while the maximum cogeneration energy efficiencies of the whole system and the ORC unit were found at 62% and 93%, respectively. Furthermore, when the oil temperature was about 150 °C, the power production rate was calculated at 2.53 kW. In addition, Bellos and Tzivanidis [13] analyzed a solar-powered trigeneration installation that produced electricity, heating, and cooling. It consisted of a PTC field, a thermal storage tank, an ORC unit, and a LiBr-H_2O absorption machine, which was fed by the ORC-rejected heat. The maximum achieved exergy efficiency was equal to 29.42%. Finally, the electricity, heating, and cooling loads were calculated at 177.6 kW, 972 kW, and 398.8 kW, respectively, for the optimum scenario.

In parallel, hydrogen has gained further attention and has been integrated into multi-generation configurations, recently. At first, hydrogen is a promising energy carrier that is not available in its molecular formula. It can be obtained from fossil fuels via hydrocarbon reforming or pyrolysis, as well as renewable sources, such as water or biomass. In addition, it can be combusted in an internal combustion engine or used in a fuel cell, while water is the only by-product of the reaction [14]. Apart from the traditional utilization in ammonia synthesis, the production of methanol, and petroleum refining, hydrogen can also be used in powering vehicles or electricity production [15]. Furthermore, hydrogen has been suggested as a solution to the energy storage problem because of the production fluctuations of renewable energy sources. Although this element has a high gravimetric energy density, it has a low volumetric one, so it must be compressed at high-pressure levels or liquefied [16]. The most common methods of hydrogen generation are the steam methane reforming of natural gas, and water electrolysis, especially proton exchange membrane (PEM) water electrolysis. Finally, hydrogen is considered a carbon-free and sustainable future fuel, if it is produced from renewable sources (green hydrogen) or fossil fuels with additional carbon capture [17].

Many publications in the literature are based on cogeneration or multigeneration units and include hydrogen as a product. Al-Nimr et al. [18] analyzed a solar energy plant that was based on concentrating photovoltaic/thermal (CPVT) collectors and an ORC module with a geothermal condenser. Moreover, a water electrolyzer was integrated to produce green hydrogen associated with a storage unit and a PEM fuel cell. The utilization of ORC led to increased overall electrical efficiency by 15.72–17.78%, compared to the case of using concentrated photovoltaics (CPV) only. In November, the overall system

efficiency was calculated at 18.21–21.95%, while the photovoltaic cell's efficiency was found at 21.96% when the ORC was utilized as a waste recovery system. In addition, Atiz et al. [19] proposed a configuration powered by PTC and a geothermal source that produced electricity and hydrogen. That system also contained an ORC and a PEM water electrolyzer. The system energy efficiency was calculated at 5.85%, the corresponding exergy efficiency was determined at 8.27%, and the total hydrogen production rate was defined at 9807.1 g/day. Finally, Khanmohammadi et al. [20] analyzed a polygeneration installation. The provided useful outputs are electricity, cooling, and hydrogen. It consisted of a flat plate collector, an ORC unit, an absorption cooling unit, and a PEM water electrolyzer. Through the optimization, overall exergy efficiency could be improved by 1.72–3.2%, and the overall cost rate was equal to 22.28 $/h.

In the present study, a solar-powered cogeneration unit that gives power and green hydrogen is investigated. The unit is based on a PTC field combined with a thermal energy storage tank, and also contains an ORC module. Moreover, the system contains a PEM water electrolyzer, which is fed with the power produced by the ORC generator, a hydrogen compression unit, and a hydrogen storage tank. This study is an innovative one because the configuration is focused on partial electricity storage in the form of hydrogen by investigating different cogeneration scenarios for determining the optimum storage strategy. More specifically, the excess electricity production by the ORC module can be utilized for hydrogen production later use, promoting the overall system flexibility. The rest electricity can be provided to the national grid, and the compressed hydrogen can be sold as a fuel. This kind of system contributes to the increasing need for the storage of surplus renewable energy and it makes possible the higher penetration on the grid of the low-grade renewable electricity production systems. It is also suitable for independent energy systems, such as in remote areas or islands. The configuration is studied parametrically, determining the proper energetic, and exergetic evaluation rates, such as overall energetic and exergetic efficiency, as well as economic indexes, such as the payback period and net present value. Especially, the calculation of the aforementioned financial indexes is an innovative process in this kind of configuration. In addition, there is a lack of studies analyzing the storage capacity and the effect of electrolyzer input power share in a PTC-based energy system, according to financial, energetic, and exergetic criteria. Finally, the analysis is performed in steady-state operating conditions, and the simulation is carried out via the Engineering Equation Solver (EES) software.

2. Material and Methods

2.1. Configuration Description

The heat input source of the examined unit is solar irradiation exploited by PTC. The collectors are installed in a North-South axis direction, while an East-West axis tracker is utilized. Taking into consideration the expected temperature values, Therminol VP-1 is considered a proper heat transfer fluid. This oil can be utilized for temperature levels from 12 °C up to 400 °C [21]. The heat that has been absorbed by the oil, is then stored in a thermal energy storage tank. The heated oil after the collector field enters the higher part of the storage tank. Moreover, the thermal oil leaves the upper part from the other side to fuel a regenerative ORC through a heat recovery system. The electricity produced by the ORC generator is crucial to providing the necessary power input to the PEM electrolyzer. The oil after the heat recovery system and before returning to the storage tank preheats water which is fed to the electrolyzer [22]. The product of this device is highly pure hydrogen, as the purity that can be achieved by water electrolysis is over 99.999% [23]. Subsequently, the hydrogen is compressed, then cooled down to the ambient conditions, and finally stored in a storage tank. As a result, the compressed hydrogen can be sold as green fuel or introduced to the gas network. The production of green hydrogen via water electrolysis to store energy for future use, when there is an amount of excess electricity, is the main purpose of the present unit. The examined cogeneration unit is depicted in Figure 1.
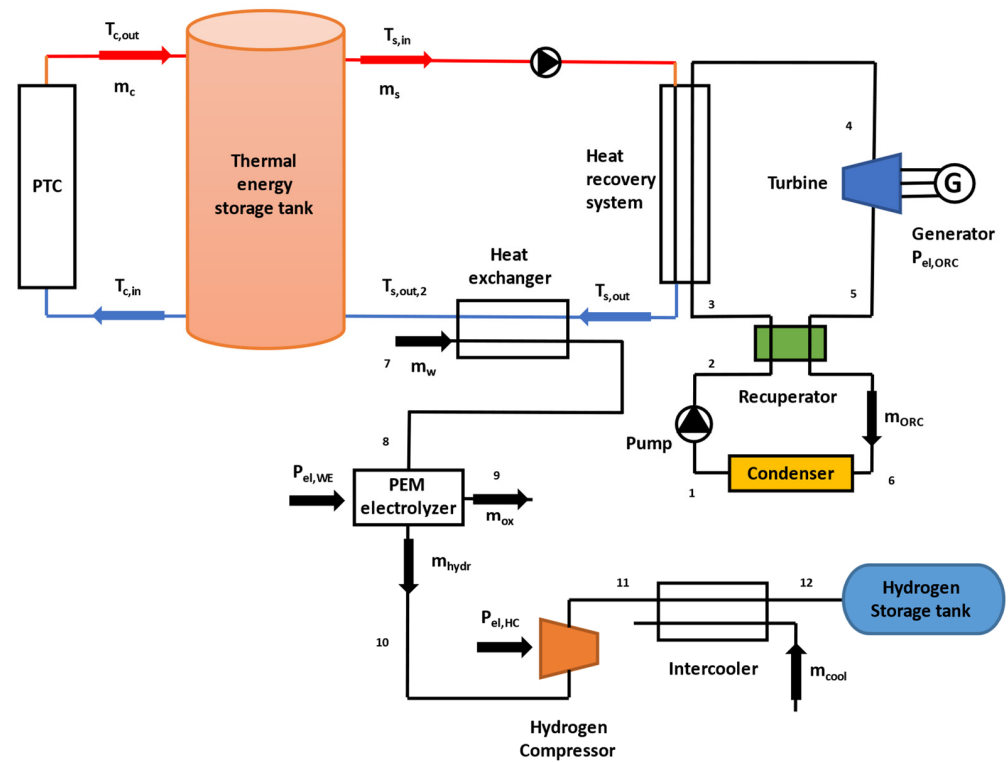
Figure 1. Solar-driven cogeneration system that produces electricity and hydrogen.

2.2. PTC Modeling

For the present installation, the parabolic collector LS-2 is used, which is a commonly investigated device in the literature. The basic geometric values are the module width, which is equal to 5 m, and the module length, which is about 7.8 m, so a module aperture of 39 m^2 is determined. Moreover, the absorber tube's outer diameter is about 70 mm, the concentration ratio is about 22.74, and the maximum optical efficiency is equal to 73.3% [24]. Other geometrical and optical parameters can be found in Ref. [24], as well as the basic thermal modeling of the collector can be found in Ref. [24]. PTCs can exploit solar beam irradiation (G_{bn}), so the available solar irradiation (Q_{solar}) is calculated as [24]:

$$Q_{solar} = A_a \cdot G_{bn} \tag{1}$$

The value (A_a) is the collector aperture. In addition, the useful heat that is taken by the working fluid is defined as [24]:

$$Q_u = \dot{m}_c \cdot c_{p,oil} \cdot (T_{c,out} - T_{c,in}) \tag{2}$$

For the collector mass flow rate, the following estimation is considered, according to Ref. [13]:

$$\dot{m}_c = 0.02 \cdot A_a \tag{3}$$

The incident angle modifier ($K(\theta)$) for the LS-2 PTC, considering the solar incident angle (θ) in degrees, can be determined as below [24]:

$$K(\theta) = \cos(\theta) + 0.000884 \cdot \theta - 0.00005369 \cdot \theta^2 \tag{4}$$

In Ref. [25], other important expressions can be found which describe the heat convection inside the tube, also the heat losses between the absorber and the cover as well as

between the cover and the ambient. The energy balance of the thermal energy storage tank is expressed by the following equation [26]:

$$Q_{st} = Q_u - Q_{in} - Q_{loss} \tag{5}$$

More specifically, the stored thermal energy (Q_{st}) is equal to the heat input to the tank, which is equal to the collector's useful heat (Q_u), minus the heat outputs from the tank, that are the heat transferred to the organic Rankine cycle system (Q_{in}) and the heat losses to the ambient (Q_{loss}). It is assumed that the storage tank does not store heat on the steady-state calculations and the thermal oil temperature is uniform in the entire tank volume. The tank heat loss coefficient (U_T) value is considered at 0.5 W/m^{2}K [13].

2.3. ORC Modeling

Through the heat recovery system, the thermal oil transfers heat to the organic medium. The heat recovery device consists of the economizer, the evaporator, and the superheater, where the fluid is converted to saturated liquid, saturated vapor, and superheated vapor, respectively. The pinch point (PP) in the inlet of the evaporator is assumed at 10 K [26] and the superheating (ΔT_{sh}) of 5 K [13] is considered. The heat recovery system modeling is illustrated in Figure 2. To make this diagram clear, it is important to state that T_3, T_{33}, and T_{34} are the organic medium temperature levels at the entrance of the economizer, evaporator, and superheater, respectively, while T_4 is the temperature level when the organic fluid exits the superheater.
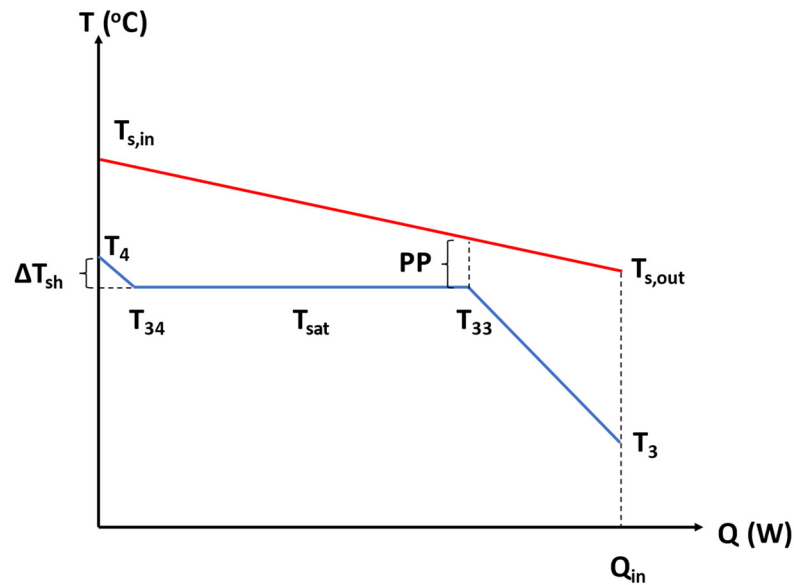

Figure 2. ORC heat recovery system modeling.

To avoid the two curves coming close, a minimum and a maximum heat recovery system inlet temperature ($T_{s,in}$) are considered by the following expressions taking into account the pinch point and the ORC fluid saturation temperature (T_{sat}) [13].

$$T_{s,in,min} = T_{sat} + PP + \Delta T_{sh} \tag{6}$$

$$T_{s,in,max} = T_3 + PP + (T_{sat} - T_3) \cdot \frac{(h_4 - h_3)}{(h_{33} - h_3)} \tag{7}$$

Based on these two values above, a dimensionless parameter (b) is assumed to define the inlet temperature as below [13]:

$$b = \frac{T_{s,in} - T_{s,in,min}}{T_{s,in,max} - T_{s,in,min}} \tag{8}$$

The parameter b is considered to be equal to zero, because the ORC achieves higher energy and exergy efficiency in this case, according to Ref. [13]. The heat input to the organic Rankine cycle (Q_{in}) is given as follows:

$$Q_{in} = \dot{m}_{ORC} \cdot (h_4 - h_3) = \dot{m}_s \cdot c_{p,oil} \cdot (T_{s,in} - T_{s,out}) \tag{9}$$

Moreover, the ORC high-pressure (P_{high}), is considered as a share of the organic medium critical pressure (P_{crit}). The parameter (α) is a ratio that compares the high pressure with the critical pressure and is defined below [26]:

$$\alpha = \frac{P_{high}}{P_{crit}} \tag{10}$$

The electricity demand of the ORC pump is defined as:

$$P_{pump} = \frac{\dot{m}_{ORC} \cdot (h_2 - h_1)}{\eta_{motor}} \tag{11}$$

The electricity production of the ORC turbine is defined as:

$$P_{turb} = \eta_{mg} \cdot \dot{m}_{ORC} \cdot (h_4 - h_5) \tag{12}$$

The net ORC electricity product is calculated as:

$$P_{el,ORC} = P_{turb} - P_{pump} \tag{13}$$

The ORC thermal efficiency is equal to:

$$\eta_{ORC} = \frac{P_{el,ORC}}{Q_{in}} \tag{14}$$

Table 1 includes all the ORC parameters of the ORC [13,26]. Taking into consideration the heat source's possible temperature levels, organic working fluids with critical temperatures in a range from 200 to 300 °C are selected. Toluene, MDM, cyclohexane, n-heptane, and n-octane are examined as high-efficient and commonly-used fluids, according to Refs. [11,13].

Table 1. ORC parameters.

Parameters of ORC	Values
Heat recovery system pinch point (PP)	10 K
Temperature difference of the recuperator (ΔT_{rec})	5 K
Temperature difference of the ORC condenser	10 K
Superheating (ΔT_{sh})	5 K
Pump's Isentropic efficiency ($\eta_{is,pump}$)	0.8
Efficiency of the pump motor (η_{motor})	0.8
Isentropic efficiency of the turbine ($\eta_{is,turb}$)	0.85
Electromechanical efficiency (η_{mg})	0.97

2.4. PEM Water Electrolyzer Modeling

At this point, the thermodynamic analysis of the PEM water electrolyzer is presented, which also includes an electrochemical model to describe the performance properly. Both electricity and thermal energy are needed for the water electrolysis process. A portion of the ORC power production is provided to the PEM water electrolyzer ($P_{el,WE}$). First of all, the total energy (ΔH) that is needed for hydrogen production is given generally through the following equation [27]:

$$\Delta H = \Delta G + T \cdot \Delta S \tag{15}$$

(ΔG) is Gibb's free energy and ($T \cdot \Delta S$) represents the thermal energy demand. The flow rate of the produced hydrogen ($\dot{N}_{hydr}$) in mol/s is calculated below [28]:

$$\dot{N}_{hydr} = \frac{J}{2 \cdot FC} = \dot{N}_{w,reacted} \tag{16}$$

In the above expression, J is the current density expressed in [A/m^2], FC is the Faraday constant, and $\dot{N}_{w, reacted}$ is the molar flow rate of reacted water. In addition, the molar flow rate of oxygen and water outlet are described by the equations below [28]:

$$\dot{N}_{ox} = \frac{J}{4 \cdot FC} \tag{17}$$

$$\dot{N}_{w,out} = \dot{N}_{w,in} - \frac{J}{2 \cdot FC} \tag{18}$$

Moreover, the hydrogen fuel exergy rate (ex_{hydr}) is calculated as [28]:

$$ex_{hydr} = ex_{hydr,chem} + ex_{hydr,phy} \tag{19}$$

($ex_{hydr,chem}$) and ($ex_{hydr,phy}$) are chemical and physical exergy rates in kJ/mol, respectively. The hydrogen chemical exergy is considered to be 236.1 kJ/mol [29]. The physical exergy can be defined as below [28]:

$$ex_{hydr,phy} = (h - h_0) - T_0 \cdot (s - s_0) \tag{20}$$

Enthalpy (h) and entropy (s) are calculated for the water electrolysis conditions, and the subscript "0" indicates the reference ambient conditions. The electricity input to the electrolyzer can be described below [28]:

$$P_{el,WE} = J \cdot V \tag{21}$$

The cell potential is the sum of the reversible potential (V_0), the activation overpotential of the anode ($V_{act,an}$), the activation overpotential of the cathode ($V_{act,cath}$), and the ohmic overpotential of the electrolyte (V_{ohm}). It is determined by the following expression [28]:

$$V = V_0 + V_{act,an} + V_{act,cath} + V_{ohm} \tag{22}$$

The reversible potential (V_0) is defined by the Nernst equation [27]:

$$V_0 = 1.229 - 8.5 \cdot 10^{-4} \cdot (T_{WE} - 298.15) \tag{23}$$

where (T_{WE}) is the temperature of the PEM electrolyzer and the membrane. The activation overpotential of the electrodes (anode, cathode) is calculated as [28]:

$$V_{act,an} = \frac{R_g \cdot T_{WE}}{FC} \cdot \sinh^{-1}\left(\frac{J}{2J_{0,an}}\right) \tag{24}$$

$$V_{act,cath} = \frac{R_g \cdot T_{WE}}{FC} \cdot \sinh^{-1}\left(\frac{J}{2J_{0,cath}}\right) \tag{25}$$

Exchange current densities, ($J_{0,an}$) and ($J_{0,cath}$), are defined by the following expressions [28]:

$$J_{0,an} = J_{an}^{ref} \cdot \exp\left(-\frac{E_{act,an}}{R_g \cdot T_{WE}}\right) \tag{26}$$

$$J_{0,cath} = J_{cath}^{ref} \cdot \exp\left(-\frac{E_{act,cath}}{R_g \cdot T_{WE}}\right) \tag{27}$$

(J_{an}^{ref}) and (J_{cath}^{ref}) are the pre-exponential factors, while ($E_{act,an}$) and ($E_{act,cath}$) is the activation energy for the anode and cathode, respectively. Furthermore, the ohmic over-potential represents the resistance of the PEM to the hydrogen cations passing through it. The membrane ionic resistance is dependent on the degree of moisture, the thickness of the membrane, and the PEM temperature. So, the local ionic conductivity σ(x) of the membrane can be described as [28]:

$$\sigma[\lambda(x)] = [0.5139 \cdot \lambda(x) - 0.326] \cdot \exp\left[1268 \cdot \left(\frac{1}{303} - \frac{1}{T_{WE}}\right)\right] \tag{28}$$

The distance (x) is counted from the cathode-membrane interface, and λ(x) is the water content at location x. This value is defined by the following equation [28]:

$$\lambda(x) = \frac{\lambda_{an} - \lambda_{cath}}{L} \cdot x + \lambda_{cath} \tag{29}$$

In Equation (29), (L) is the membrane thickness, (λ_{an}) and (λ_{cath}) are the moisture contents at the anode-membrane and the cathode-membrane interface, respectively. Thus, the overall PEM ohmic resistance (R_{PEM}) is calculated below [28]:

$$R_{PEM} = \int_0^L \frac{dx}{\sigma[\lambda(x)]} \tag{30}$$

So, the PEM ohmic overpotential is defined as [28]:

$$V_{ohm} = J \cdot R_{PEM} \tag{31}$$

The overpotentials lead to entropy generation σ, which is calculated as [28]:

$$\sigma = 2 \cdot FC \cdot (V_{act,an} + V_{act,cath} + V_{ohm}) \tag{32}$$

For σ ≥ T·ΔS, the heat produced because of the irreversibilities is equal to or higher than the required heat for the electrolysis. So, external heat is not needed for the PEM electrolyzer, and $Q_{heat,WE} = Ex_{heat,WE} = 0$. If σ < T·ΔS, the generated heat is lower than the needed heat. So, the heat input to the PEM electrolyzer is given as follows [28]:

$$Q_{heat,WE} = [T \cdot \Delta S - \sigma] \cdot \dot{N}_{w,reacted} = \frac{J}{2FC} \cdot [T \cdot \Delta S - \sigma] \tag{33}$$

The corresponding exergy rate of the heat input to the electrolyzer is calculated by the following expression [28]:

$$Ex_{heat,WE} = Q_{heat,WE} \cdot \left(1 - \frac{T_o}{T_{WE}}\right) \tag{34}$$

The heat required to preheat the incoming water up to (T_{WE}) is defined as ($Q_{heat,w}$) and the corresponding exergy rate as ($Ex_{heat,w}$).

All the parameters of the PEM water electrolyzer are included in Table 2 [28,29]. It is essential to state that the selected pressure of 1 bar is the most conventional option, according to the literature [30].

Table 2. Parameters of the PEM water electrolyzer modeling.

Parameters	Values
Oxygen pressure (P_{ox})	1.0 bar
Hydrogen pressure (P_{hydr})	1.0 bar
PEM water electrolyzer temperature (TWE)	80 °C (353.15 K)
Reference temperature (T_0)	25 °C (298.15 K)
Activation energy of the anode reaction ($E_{act,an}$)	76 kJ/mol
Activation energy of the cathode reaction ($E_{act,cath}$)	18 kJ/mol
Water content at the anode-membrane interface (λ_{an})	14 Ω^{-1}
Water content at the cathode-membrane interface (λ_{cath})	10 Ω^{-1}
Thickness of the membrane (L)	100 μm
Gas constant (R_g)	8.314 J/mol·K
Faraday constant (FC)	96,485.3 s·A/mol
Hydrogen low heating value (LHV_{hydr})	120 MJ/kg
Hydrogen chemical exergy ($Ex_{hydr,chem}$)	236.1 kJ/mol

2.5. Hydrogen Compression and Storage System Modeling

After the electrolysis process, hydrogen is compressed up to the pressure level of 100 bar [31]. A portion of ORC power production is utilized to compress the hydrogen into the proper pressure level to be sold as compressed hydrogen fuel for later use. So, the electricity consumption rate of the hydrogen compressor is described below:

$$P_{el,HC} = \frac{\dot{m}_{hydr} \cdot (h_{11,is} - h_{10})}{\eta_{is,comp} \cdot \eta_{mg}} \tag{35}$$

The isentropic efficiency of the hydrogen compressor $\eta_{is,comp}$ is considered at 85%. Because of the compression, hydrogen achieves high-temperature levels, so cooling is needed. Then, the hydrogen is stored in a tank at a pressure of 100 bar and a temperature of 25 °C [31]. In all the examined cases, a hydrogen storage tank of 10 kg is selected.

2.6. Overall Installation Indexes

The net electricity production of the whole installation ($P_{el,net}$) can be defined by the following expression:

$$P_{el,net} = P_{el,ORC} - P_{el,WE} - P_{el,HC} \tag{36}$$

The overall system's energetic performance (η_{en}) is calculated as:

$$\eta_{en} = \frac{P_{el,net} + LHV_{hydr} \cdot \dot{m}_{hydr}}{Q_{solar}} \tag{37}$$

The overall system's exergetic performance (η_{ex}) is calculated as:

$$\eta_{ex} = \frac{Ex_{el,net} + ex_{hydr} \cdot \dot{N}_{hydr}}{Ex_{solar}} \tag{38}$$

The exergy rate of net electricity production ($Ex_{el,net}$) is equal to the corresponding energy rate ($P_{el,net}$). The solar exergy rate is described based on the Petela model by the following equation [26]:

$$Ex_{solar} = Q_{solar} \cdot \left(1 - \frac{4}{3} \cdot \frac{T_0}{T_{sun}} + \frac{1}{3} \left(\frac{T_0}{T_{sun}} \right)^4 \right) \tag{39}$$

The reference temperature (T_0) is defined at 298.15 K (25 °C) and the sun temperature (T_{sun}) at 5770 K [26]. Similarly, the overall energy and exergy efficiency can be also described on an annual basis taking into account the performance during the year.

2.7. Financial Evaluation

The investment cost of the cogeneration unit (C_0) consists of the cost of the PTCs, the thermal energy storage tank, the organic Rankine cycle, the PEM water electrolyzer, the hydrogen compressor, the hydrogen storage tank, and the heat exchangers (water preheater and hydrogen cooler). It is expressed below:

$$C_0 = C_{PTC} + C_T + C_{ORC} + C_{WE} + C_{HC} + C_{HST} + C_{HEX} \tag{40}$$

In addition, the annual cash flow (CF) is determined assuming the annual inflows and outflows. The annual inflows are defined as the income from electricity and green hydrogen production, while the annual outflows include the operation and maintenance costs.

$$CF = Y_{el} \cdot K_{el} + Y_{hydr} \cdot K_{hydr} - K_{O\&M} \tag{41}$$

In the previous equation, (Y_{el}) is the yearly electricity production in kWh, (Y_{hydr}) is the yearly hydrogen generation in kg, and (K_{hydr}) is the selling cost of hydrogen in €/kg. Furthermore, the simple payback period (SPBP) is calculated as:

$$SPBP = \frac{C_0}{CF} \tag{42}$$

The payback period (PBP) is calculated as:

$$PBP = \frac{\ln\left(\frac{CF}{CF - C_0 \cdot i}\right)}{\ln(1 + i)} \tag{43}$$

The net present value (NPV) is calculated as:

$$NPV = -C_0 + CF \cdot \frac{(1 + i)^N - 1}{i \cdot (1 + i)^N} \tag{44}$$

The internal rate of return (IRR) is determined by solving the following non-linear equation:

$$IRR = \frac{CF}{C_0} \cdot \left(1 - \frac{1}{(1 + IRR)^N}\right) \tag{45}$$

The aforementioned financial parameters are presented in Table 3.

Table 3. Financial analysis parameters.

Financial Parameters	Values
PTC specific cost	230 €/m^2 [32]
Thermal energy storage tank specific cost	1000 €/m^3 [26]
ORC specific cost	1800 €/kW$_{el}$ [32]
PEM water electrolyzer specific cost	800 €/kW$_{el}$ [33]
Hydrogen storage tank specific cost	600 €/kg [31,34]
Hydrogen compressor specific cost	1600 €/kW$_{el}$ [31]
Heat exchanger specific cost	100 €/kW [26]
Project lifetime (N)	25 years [32]
Discount factor (i)	4% [26]
Operation & maintenance cost ($K_{O\&M}$)	2% of the capital cost [32]
Cost of electricity (K_{el})	0.30 €/kWh [35]

2.8. Simulation Methodology

The analysis for both thermodynamic and financial calculations is performed in steady-state conditions and carried out in the EES software, which solves non-linear equations and contains a large properties database of numerous working fluids. So, the EES software

database is used for the thermodynamic properties of all the examined working media. The aforementioned developed models have been validated by the same research team considering experimental data in Ref. [35].

The cogeneration unit is located in Athens, Greece. The solar field consists of 5 modules of the LS-2 PTC, so the collector aperture (A_a) is equal to 195 m^2. Furthermore, the thermal energy storage tank volume (V_T) is defined by the ratio of the collector aperture to the storage volume $\left(\frac{A_a}{V_T} \right)$. This parameter is used in the literature and a typical value, that is assumed in this study, is equal to 80 [13,32].

The simulation is conducted by taking into account a solar irradiation value that is equal to 700 W/m^2, a solar incident angle of 30°, and an ambient temperature of 25 °C. Moreover, the configuration operates only on sunny days, so for the location of Athens, the operating hours are assumed to be 2500 per year. According to Ref. [36], if the steady-state simulation is performed in the aforementioned conditions, the results are similar to the results of a detailed dynamic analysis, for a concentrated solar power plant in Athens. So, these values are used to estimate all the important outputs, including the financial indexes. In parallel, it is important to mention that no significant degradation of the PEM water electrolyzer is expected, as the system is assumed to operate 62,500 h during the 25-year lifetime. It is estimated that the electrolyzer efficiency decreases by almost 1.1% over 10,000 operating hours [37].

At first, the analysis is focused on the organic working fluid selection based on the ORC exergy efficiency. Furthermore, a parametric analysis is performed and split into two sections, the thermodynamic and the financial one. The examined thermodynamic parameters are the share of ORC electricity production that powers the PEM water electrolyzer, as well as the solar beam irradiation value, which varies from 500 to 900 W/m^2, with a step that is equal to 200 W/m^2. The main financial parameter is the selling price of hydrogen, which varies from 5 to 15 €/kg [38]. After the parametric analysis, it is essential to define a final system design through a simple optimization process. To carry out this analysis, a dimensional criterion is considered, which includes two thermodynamic objectives, i.e., the maximum overall system exergy efficiency and the maximum hydrogen production. Through this criterion, a design case that produces a significant amount of hydrogen without a sizeable reduction in the exergy performance is determined. According to the criterion, the selected final point is the one that is closest to the ideal point, where the two objectives are optimized at the same time. For this case, the dimensional criterion (F) is expressed by the following equation [26]:

$$F = \sqrt{ \left(\frac{\eta_{ex} - \eta_{exmax}}{\eta_{exmax} - \eta_{exmin}} \right)^2 + \left(\frac{\dot{m}_{hydr} - \dot{m}_{hydrmax}}{\dot{m}_{hydrmax} - \dot{m}_{hydrmin}} \right)^2 } \tag{46}$$

3. Results and Discussion

3.1. Preliminary Analysis

At first, the investigation is concentrated on the selection of the most proper working medium for the organic cycle. So, the ORC energy efficiency, the ORC electricity production, as well as the overall exergy efficiency are determined for different working fluids considering various ORC high-pressure values. The high pressure varies though changing the parameter (α) which is the ratio of the ORC high pressure to the critical pressure of the medium in a range from 0.2 to 0.9 [26]. The system exergy efficiency is defined taking into account that the electrolyzer is out of order, so the configuration operates as a power plant. According to the results that are illustrated in Figures 3–5, in the cases of using MDM, toluene, or n-octane, greater values of the ORC energy efficiency, the ORC electricity production, and the exergy efficiency are achieved. However, the selection criterion has been decided to be the overall exergy performance. More specifically, the total maximum exergy efficiency is achieved utilizing MDM as the working fluid, while the parameter (α) is equal to 0.9. In this operation scenario, the ORC electricity production is equal to

24.776 kW, while the overall energy and exergy efficiency is determined at 18.15% and 19.49%, respectively. So, MDM is selected as the most proper working fluid for this case study. This fluid is an appropriate choice for the examined heat source temperature level. The most important parameters and outputs are presented in Tables 4 and 5, respectively.
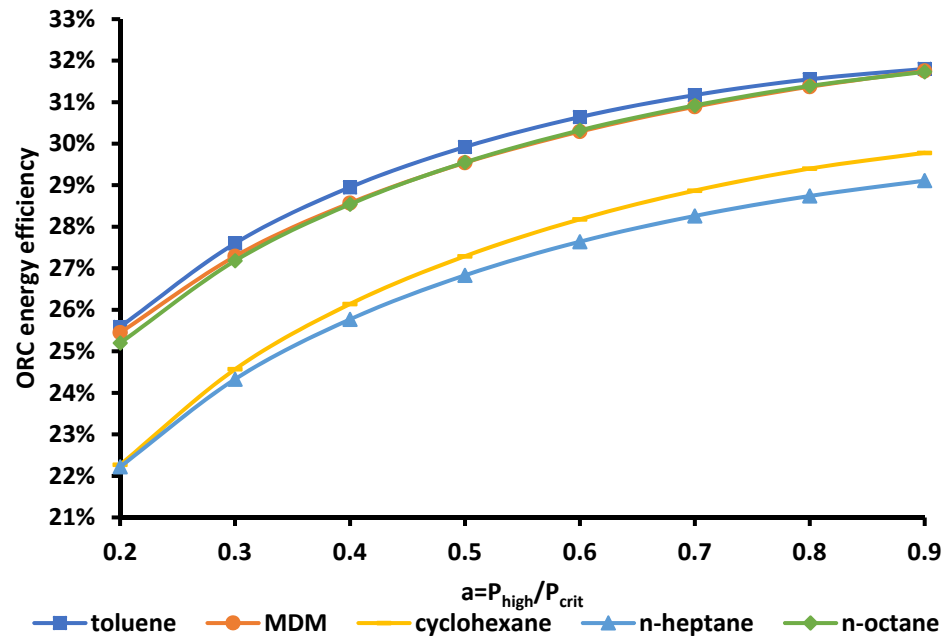

Figure 3. ORC energy efficiency depending on the parameter (α) for different working fluids.
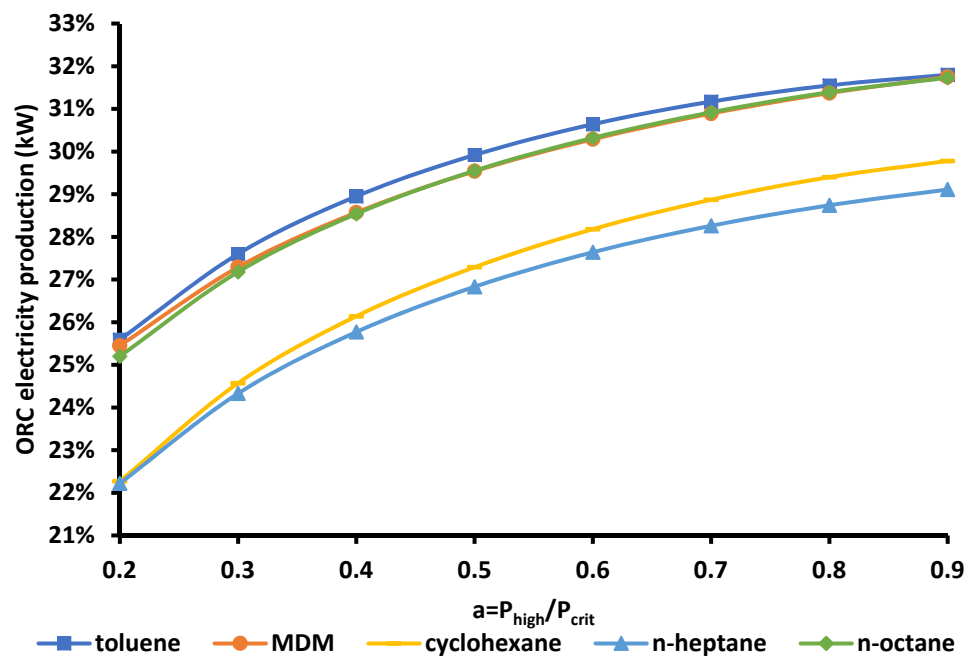

Figure 4. ORC electricity production depending on the parameter (α) for different working fluids.
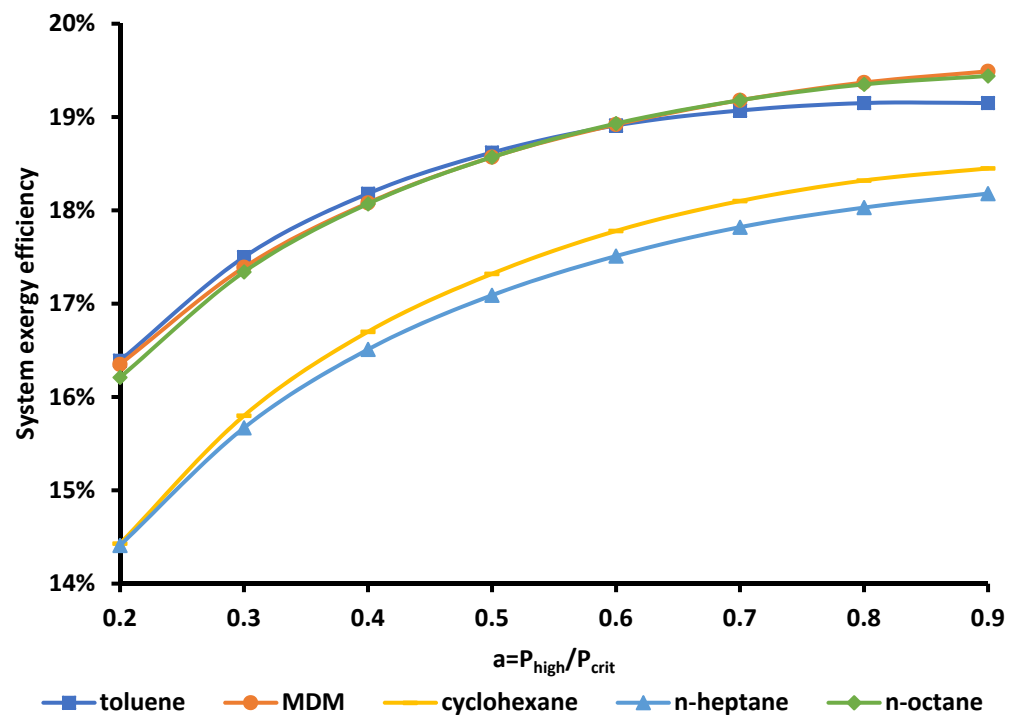
Figure 5. Overall system exergy efficiency depending on the parameter (α) for different working fluids, considering only electricity production through the ORC.

Table 4. Design parameters of the system.

Parameters	Values
Design ambient temperature (T_{amb})	25 °C
Solar beam irradiation (G_{bn})	700 W/m^2
Incident angle (θ)	30°
Collector aperture (A_a)	195 m^2
Ratio of collector aperture to the tank volume ($\frac{A_a}{V_T}$)	80 m^2/m^3
Ratio of the ORC high pressure to the critical pressure (α)	0.9
Heat recovery system inlet temperature definition parameter (b)	0

Table 5. System outputs when only electricity is produced.

Outputs	Values
Solar energy input (Q_{solar})	136.5 kW
ORC heat input (Q_{in})	78.04 kW
ORC electricity production ($P_{el,ORC}$)	24.78 kW
ORC thermal efficiency (η_{ORC})	31.75%
System energy efficiency (η_{en})	18.15%
System exergy efficiency (η_{ex})	19.49%

3.2. Parametric Analysis of the System

3.2.1. Thermodynamic Parametric Analysis

For the thermodynamic calculations, the parameters that are taken into account are the electricity input to the electrolyzer and the solar beam irradiation. When the default irradiation value of 700 W/m^2 is considered, the PEM electrolyzer power input varies from 0 to 22.92 kW, which is the case when the whole ORC electricity production is used to power the PEM water electrolyzer and the hydrogen compressor, so there is no net electricity generation. Consequently, the main plant outputs, which are the net electricity production, the overall system energy, and exergy efficiency, are included in this section,

depending on the electrolyzer power input and the solar beam irradiation. As it is shown in Figure 6, the net electricity generation has a linear decreasing rate depending on the electricity input to the electrolyzer. The maximum value is equal to 17.15 kW when solar beam irradiation is equal to 500 W/m², 24.78 kW when this value is equal to 700 W/m², and 32.40 kW when this value is equal to 900 W/m². These are the cases of zero hydrogen production and compression, while the minimum values are equal to zero when the installation does not provide electricity and the entire power is utilized for hydrogen production and compression. In Figures 7 and 8, it is illustrated that both energy and exergy efficiency decrease when the electricity feeds to the PEM water electrolyzer, and the hydrogen production rate increase. When the plant provides only electricity to the grid, the energy and exergy efficiency are determined at 18.46% and 19.83%, respectively, in the case of the solar beam irradiation that is equal to 900 W/m². However, in the case of maximum hydrogen generation, these rates are equal to 9.6% and 10.07%, respectively. Finally, according to the results, the net power production, as well as the overall energy and exergy efficiencies increase with the increase of solar beam irradiation. The calculated values of both energy and exergy efficiency are greater than the corresponding ones defined by Atiz et al. [19]. The authors of this study investigated a similar system that is based on the PTC-powered ORC, as well as provides electricity and hydrogen, leading to an energy efficiency of 5.85%, and an exergy efficiency of 8.27%. In the present work, it is assumed that both the pump and turbine achieve high isentropic efficiency, enhancing the overall ORC performance.
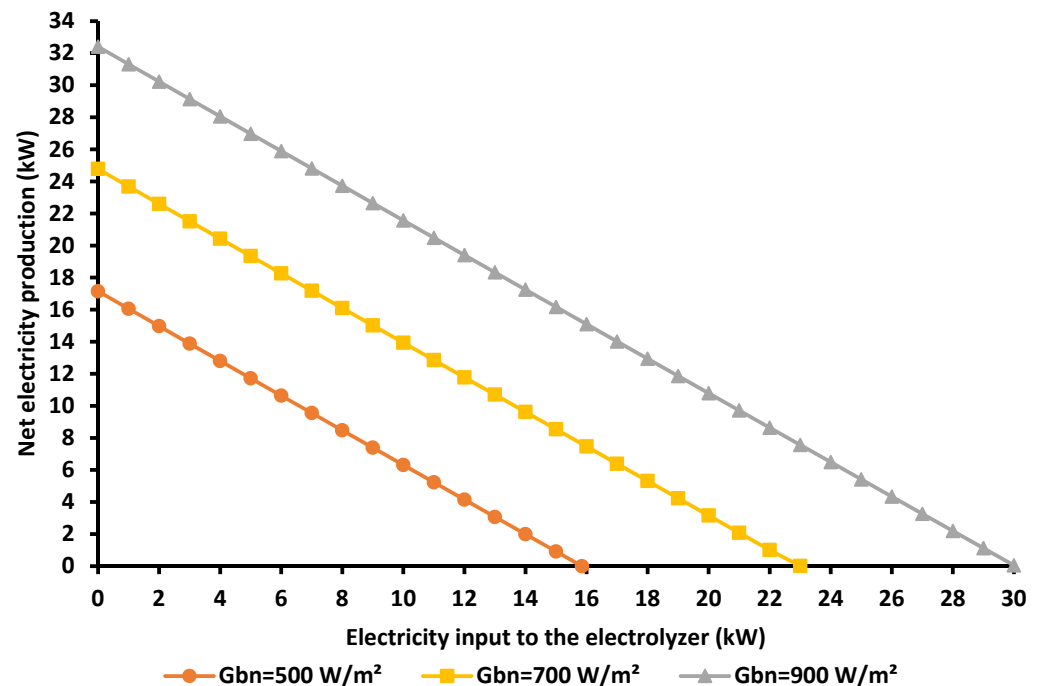

Figure 6. Net electricity production depending on the power input to the electrolyzer for different solar beam irradiation.
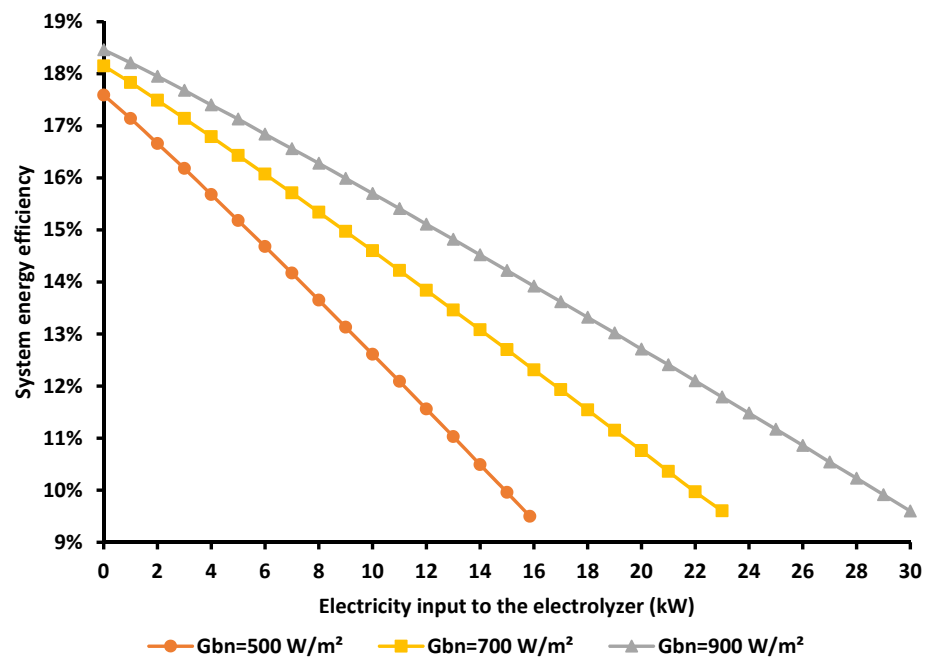
Figure 7. Overall energy efficiency depending on the electricity input to the electrolyzer for different solar beam irradiation.
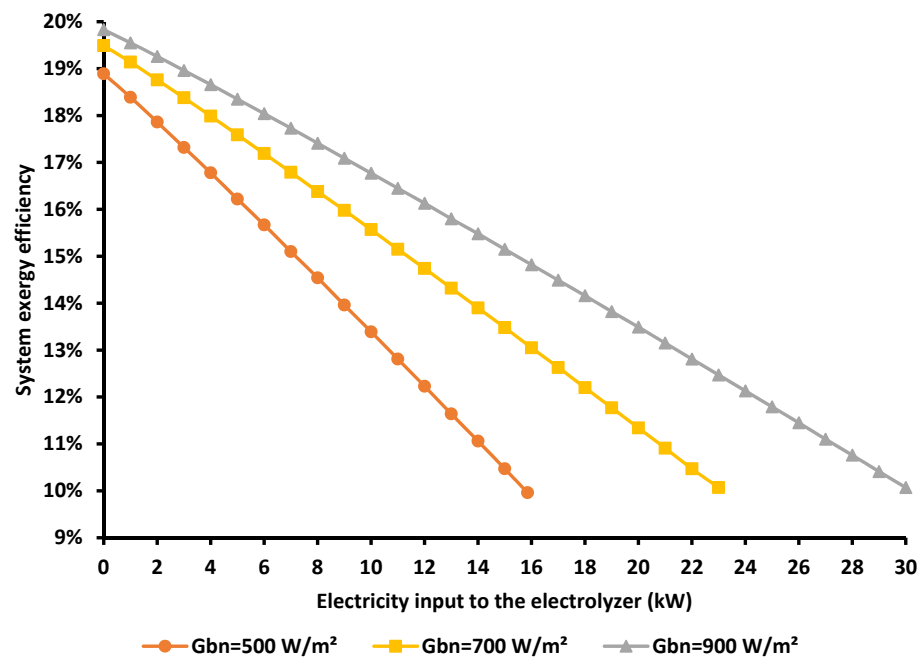

Figure 8. Overall exergy efficiency depending on the power input to the electrolyzer for different solar beam irradiation.

3.2.2. Financial Parametric Analysis

The financial analysis is carried out by approaching the transient system operation. So, a solar irradiation value that is equal to 700 W/m², a solar incident angle of 30°, an ambient temperature of 25 °C, as well as 2500 operating hours per year, are considered for this approach. Different irradiation values are not included, as the financial study is important to focus on economic parameters. The main examined parameter is the selling price of hydrogen. Considering this variation, it is possible to evaluate the system financially in different market conditions that may occur in the future. In parallel, different electricity inputs to the PEM water electrolyzer are taken into account to investigate the influence of

the hydrogen generation rate on economic viability. The fundamental financial indexes are the PBP and NPV. Figures 9 and 10 indicate that the PBP and the NPV have a decreasing and an increasing rate, respectively, depending on the hydrogen selling price. On the other hand, the PBP and the NPV decrease, when the electricity that feeds the electrolyzer and the hydrogen production increases. The highest financial performance is achieved when the electricity input to the electrolyzer is equal to 2 kW, so the PBP is calculated at 7.12 years and the NPV is determined at 156,226 € if the selling price is equal to 15 €/kg.
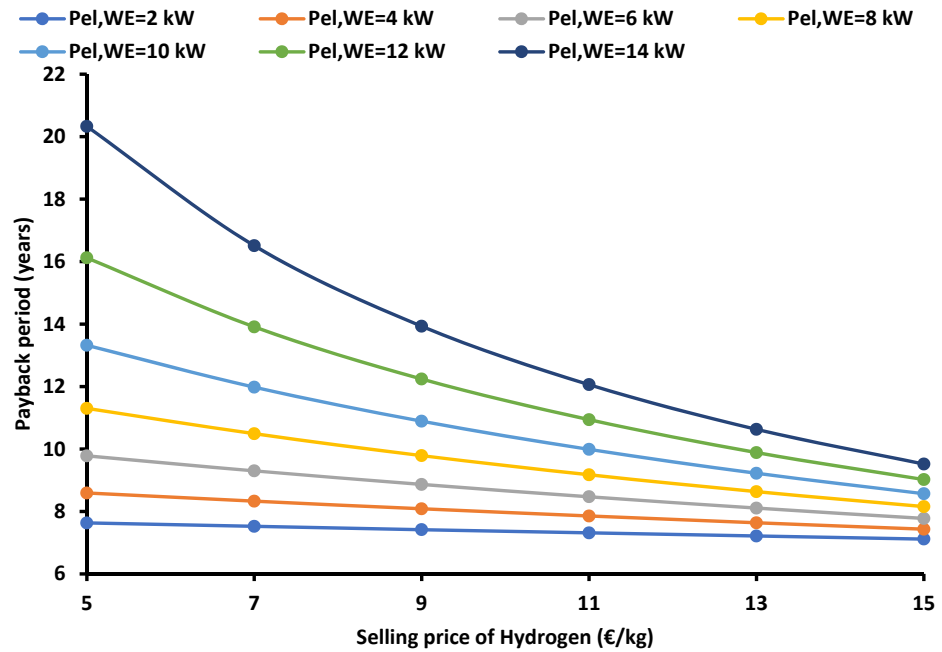

Figure 9. Payback period depending on the selling price of hydrogen for different electricity inputs to the electrolyzer.
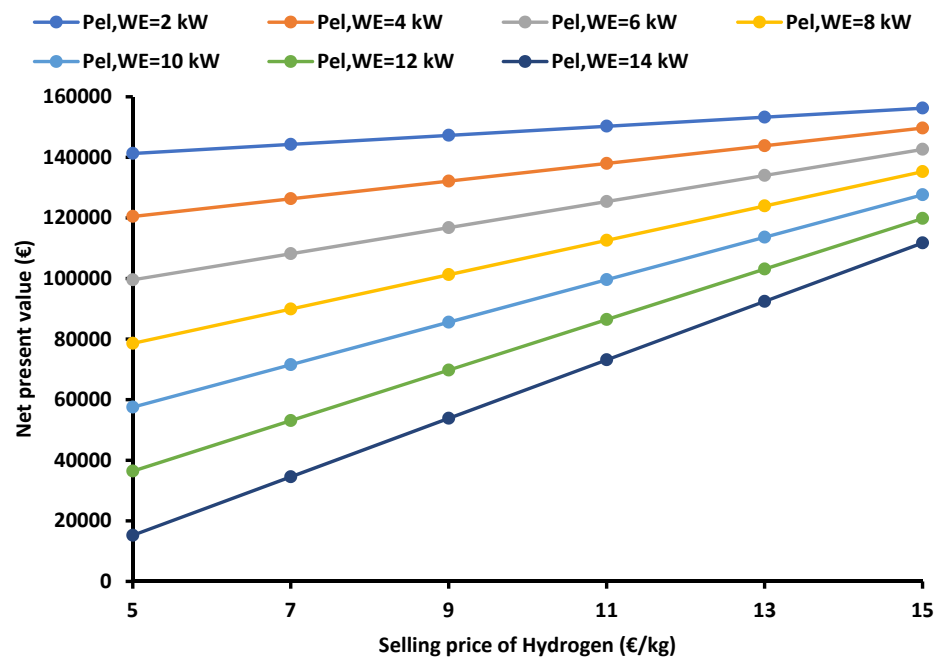

Figure 10. Net present value depending on the selling price of hydrogen for different electricity inputs to the electrolyzer.

3.3. Final System Design Based on Thermodynamic Criteria

To define the final operation scenario, the objectives assumed are the maximum possible system exergy efficiency and the maximum possible hydrogen production rate. So, the selection is based on thermodynamic criteria and leads to an operation scenario, that guarantees a basic hydrogen production amount with an acceptable configuration exergy efficiency. As it is shown in Figure 11, the dimensional criterion (F) is minimized when the electricity that is provided to the PEM water electrolyzer is equal to 11.5 kW. The rest of the electricity produced by the ORC powers the hydrogen compression facility, as well as is sold to the grid. At this point, it is essential to mention that to achieve the aforementioned criteria, almost 50% of the ORC electricity load has to feed the PEM electrolyzer. Consequently, the overall operation is balanced between the net electricity production, and the electricity load provided for hydrogen generation.
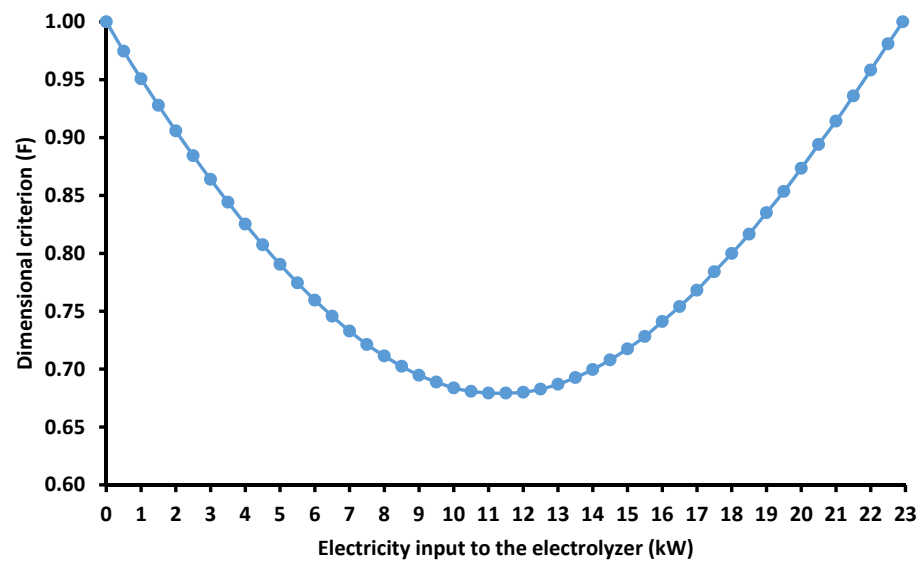

Figure 11. Dimensional criterion (F) depending on the electricity input to the electrolyzer.

For this case, the overall energy efficiency is equal to 14.03%, the exergy performance is determined at 14.94%, while the hydrogen production rate is equal to 0.205 kg/h. If the selling price of hydrogen is equal to 15 €/kg, the PBP is equal to 8.9 years, the SPBP is calculated at 7.37 years, the NPV at 121,777 €, and the internal rate of return at 12.92%. In addition, the investment cost is found at 108,726 €. The useful outputs of the final unit design are presented in Table 6. Finally, in Figure 12, the capital cost is analyzed and the share of each subsystem and component is presented. According to this diagram, the largest portion regards the PTC and ORC, with a share of 41.3% and 41%, respectively.

Table 6. Outputs of the final system design.

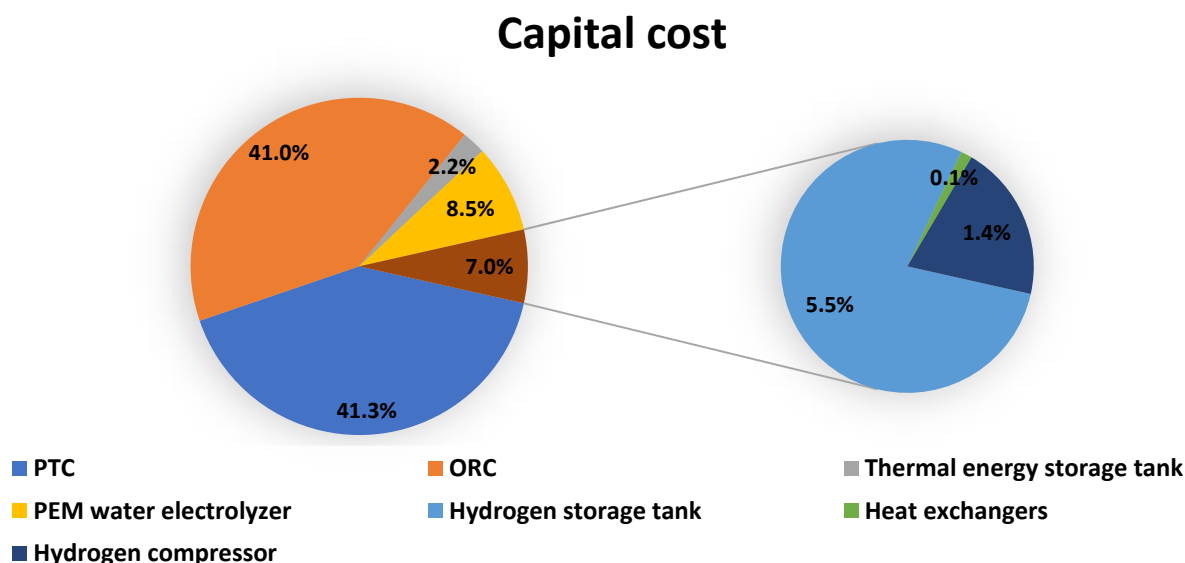| Outputs	Values
ORC electricity production ($P_{el,ORC}$)	24.78 kW
Net electricity production ($P_{el,net}$)	12.32 kW
Electricity input to the electrolyzer ($P_{el,WE}$)	11.5 kW
Electricity consumption of the hydrogen compressor ($P_{el,HC}$)	0.96 kW
Hydrogen production rate ($\dot{m}_{hydr}$)	0.205 kg/h
System energy efficiency (η_{en})	14.03%
System exergy efficiency (η_{ex})	14.94%
Capital cost (C_0)	108,726 €
Simple payback period (**SPBP**)	7.37
Payback period (**PBP**)	8.90
Internal rate of return (**IRR**)	12.92%
Net present value (**NPV**)	121,777 €

Capital cost

Figure 12. Capital cost separation into parts.

4. Conclusions

The purpose of this publication is the parametric investigation of a solar-power co-generation unit, which can produce electricity and compressed green hydrogen. The total configuration consists of a PTC field, where solar irradiation is exploited, a thermal energy storage tank, an ORC unit, a PEM water electrolyzer to produce pure hydrogen, as well as a hydrogen compression and storage system. The analysis is focused on developing a system that will achieve high thermodynamic performance and economic viability. The unit has been investigated based on the climate data of Athens, Greece, while it can also be installed in a remote area or island. The most dominant conclusions of this analysis are described below:

- MDM is selected as the most proper working fluid because achieves the highest exergy performance.
- When the power input to the electrolyzer and the hydrogen production rate increases, the net electricity generation, energy efficiency, and exergy performance decrease, while the installation is less economically viable.
- In the final unit design, the net electricity production is 12.32 kW and the electricity that feeds the electrolyzer is 11.5 kW, which leads to a hydrogen production rate of 0.205 kg/h.
- The overall unit energetic performance is 14.03% and the exergy efficiency is 14.94%.
- The PBP is calculated to be equal to 8.9 years, the NPV is 122 k€, and the IRR is 12.92%.
- The present installation promotes the goals of sustainability and green energy policies in the domain of green electricity production and energy storage.

Finally, future research should concentrate on detailed dynamic analysis and the system control strategy. In parallel, the integration of other devices to produce additional outputs, such as water heaters for useful heating or absorption chillers for cooling purposes, as well as the installation of other solar collectors, should also be examined.

Author Contributions: Conceptualization, P.L., N.G. and E.B.; methodology, P.L., A.K. and D.N.K.; software, P.L., N.G. and E.B.; validation, P.L., A.K. and D.N.K.; formal analysis, P.L. and N.G.; investigation, P.L., N.G. and E.B.; writing—original draft preparation, P.L., N.G., A.K., D.N.K., E.B. and C.T.; writing—review and editing, P.L., N.G., A.K., D.N.K., E.B. and C.T.; supervision, E.B. and C.T. All authors have read and agreed to the published version of the manuscript.

Institutional Review Board Statement: Not applicable.

Nomenclature

A_a	Collector aperture, m^2
C	Component capital cost, €
C_0	System capital cost, €
c_p	Specific heat capacity under constant pressure, J/kg·K
CF	Cash Flow, €
E_{act}	Activation energy, J/mol
ex	Specific exergy, J/kg or J/mol
Ex	Exergy rate, W
F	Objective function, -
G	Gibb's free energy, J/mol
G_{bn}	Solar beam irradiation, W/m^2
h	Specific enthalpy, J/kg or J/mol
i	Discount factor, %
J	Current density, A/m^2
K	Cost, €
$K(\theta)$	Incident angle modifier, -
L	Membrane thickness, mm
LHV	Low Heating Value, kJ/kg
$\dot{m}$	Mass flow rate, kg/s
N	Lifetime, years
$\dot{N}$	Molar flow rate, mol/s
NPV	Net Present Value, €
P	Pressure, bar
P_{el}	Electricity rate, W
PBP	Payback Period, years
Q	Energy rate, W
q	Thermal losses per collector aperture, W/m^2
R	Ohmic resistance, Ω
R_g	Gas constant, J/(mol·K)
s	Entropy, J/mol or J/kg
SPBP	Simple Payback Period, years
T	Temperature, °C or K
t	Time, s
U	Heat loss coefficient, $W/m^2 K$
u	Velocity, m/s
V	Potential, V
V_T	Thermal storage tank volume, m^3
$\dot{V}$	Volumetric flow rate, m^3/s
Y	Yearly parameter, -
Greek symbols	
Δ	Difference
η	Efficiency, -
θ	Incident angle, °
$\lambda(x)$	Water content, Ω^{-1}
ρ	Density, kg/m^3
σ	Entropy generation, J/mol
$\sigma(x)$	Local ionic conductivity of the membrane, s/m
x	Distance from the cathode-membrane interface, mm

Subscripts and superscripts

0	Reference condition
act	Activation
air	Air
amb	Ambient
an	Anode
c	Collector
cath	Cathode
chem	Chemical
comp	Compressor
cool	Coolant
crit	Critical point
el	Electricity
en	Energy
ex	Exergy
fluid	Fluid
HC	Hydrogen compressor
heat	Heating
HEX	Heat exchanger
high	High value
HST	Hydrogen storage tank
hydr	Hydrogen
in	Inlet
is	Isentropic
loss	Losses
low	Low value
max	Maximum value
mg	Electro-mechanical
min	Minimum value
motor	Motor
net	Net value
O&M	Operation and maintenance
ohm	Ohmic
oil	Thermal oil
ORC	Organic Rankine Cycle
out	Outlet
ox	Oxygen
PEM	Proton exchange membrane
phy	Physical
PTC	Parabolic trough collector
pump	Pump
reacted	Reacted
rec	Recuperator
ref	Reference
sat	Saturation
sh	Superheating
solar	Solar energy
st	Stored in the tank
sun	Sun
T	Tank
th	Thermal
turb	Turbine
u	Useful
w	Water
WE	Water electrolyzer

Abbreviations

CPV	Concentrated photovoltaic
CPVT	Concentrated photovoltaic/thermal collector
EES	Engineering Equation Solver
FC	Faraday Constant
IRR	Internal Rate of Return
ORC	Organic Rankine Cycle
PEM	Proton Exchange Membrane
PP	Pinch Point
PTC	Parabolic Trough Collector

References

1. Rao, V.T.; Sekhar, Y.R.; Pandey, A.K.; Said, Z.; Prasad, D.R.; Hossain, M.S.; Selvaraj, J. Thermal analysis of hybrid photovoltaic-thermal water collector modified with latent heat thermal energy storage and two side serpentine absorber design. *J. Energy Storage* **2022**, *56*, 105968. [CrossRef]
2. Vivek, C.; Ramkumar, P.; Srividhya, P.; Sivasubramanian, M. Recent strategies and trends in implanting of renewable energy sources for sustainability—A review. *Mater. Today Proc.* **2021**, *46*, 8204–8208. [CrossRef]
3. Mahapatra, A.; Prochowicz, D.; Tavakoli, M.M.; Trivedi, S.; Kumar, P.; Yadav, P.K. A review of aspects of additive engineering in perovskite solar cells. *J. Mater. Chem. A* **2019**, *8*, 27–54. [CrossRef]
4. Mohammadi, K.; Khanmohammadi, S.; Khorasanizadeh, H.; Powell, K. A comprehensive review of solar only and hybrid solar driven multigeneration systems: Classifications, benefits, design and prospective. *Appl. Energy* **2020**, *268*, 114940. [CrossRef]
5. Kavadias, K.A.; Kosmas, V.; Tzelepis, S. Sizing, Optimization, and Financial Analysis of a Green Hydrogen Refueling Station in Remote Regions. *Energies* **2022**, *15*, 547. [CrossRef]
6. Evangelisti, L.; Vollaro, R.D.L.; Asdrubali, F. Latest advances on solar thermal collectors: A comprehensive review. *Renew. Sustain. Energy Rev.* **2019**, *11*, 109318. [CrossRef]
7. Kasaeian, A.; Bellos, E.; Shamaeizadeh, A.; Tzivanidis, C. Solar-driven polygeneration systems: Recent progress and outlook. *Appl. Energy* **2020**, *264*, 114764. [CrossRef]
8. Bao, J.; Zhao, L. A review of working fluid and expander selections for organic Rankine cycle. *Renew. Sustain. Energy Rev.* **2013**, *24*, 325–342. [CrossRef]
9. Yu, H.; Helland, H.; Yu, X.; Gundersen, T.; Sin, G. Optimal design and operation of an Organic Rankine Cycle (ORC) system driven by solar energy with sensible thermal energy storage. *Energy Convers. Manag.* **2021**, *244*, 114494. [CrossRef]
10. Altun, A.; Kilic, M. Thermodynamic performance evaluation of a geothermal ORC power plant. *Renew. Energy* **2019**, *148*, 261–274. [CrossRef]
11. Bellos, E.; Tzivanidis, C. Investigation of a hybrid ORC driven by waste heat and solar energy. *Energy Convers. Manag.* **2017**, *156*, 427–439. [CrossRef]
12. Carraro, G.; Bori, V.; Lazzaretto, A.; Toniato, G.; Danieli, P. Experimental investigation of an innovative biomass-fired micro-ORC system for cogeneration applications. *Renew. Energy* **2020**, *161*, 1226–1243. [CrossRef]
13. Bellos, E.; Tzivanidis, C. Parametric analysis and optimization of a solar driven trigeneration system based on ORC and absorption heat pump. *J. Clean. Prod.* **2017**, *161*, 493–509. [CrossRef]
14. Tzelepis, S.; Kavadias, K.A.; Marnellos, G.E.; Xydis, G. A review study on proton exchange membrane fuel cell electrochemical performance focusing on anode and cathode catalyst layer modelling at macroscopic level. *Renew. Sustain. Energy Rev.* **2021**, *151*, 111543. [CrossRef]
15. Fan, L.; Tu, Z.; Chan, S.H. Recent development of hydrogen and fuel cell technologies: A review. *Energy Rep.* **2021**, *7*, 8421–8446. [CrossRef]
16. Olabi, A.G.; Abdelghafar, A.A.; Baroutaji, A.; Sayed, E.T.; Alami, A.H.; Rezk, H.; Abdelkareem, M.A. Large-vscale hydrogen production and storage technologies: Current status and future directions. *Int. J. Hydrogen Energy* **2021**, *46*, 23498–23528. [CrossRef]
17. Tashie-Lewis, B.C.; Nnabuife, S.G. Hydrogen Production, Distribution, Storage and Power Conversion in a Hydrogen Economy—A Technology Review. *Chem. Eng. J. Adv.* **2021**, *8*, 100172. [CrossRef]
18. Al-Nimr, M.D.A.; Bukhari, M.; Mansour, M. A combined CPV/T and ORC solar power generation system integrated with geothermal cooling and electrolyser/fuel cell storage unit. *Energy* **2017**, *133*, 513–524. [CrossRef]
19. Atiz, A.; Karakilcik, H.; Erden, M.; Karakilcik, M. Assessment of power and hydrogen production performance of an integrated system based on middle-grade geothermal source and solar energy. *Int. J. Hydrogen Energy* **2020**, *46*, 272–288. [CrossRef]
20. Khanmohammadi, S.; Heidarnejad, P.; Javani, N.; Ganjehsarabi, H. Exergoeconomic analysis and multi objective optimization of a solar based integrated energy system for hydrogen production. *Int. J. Hydrogen Energy* **2017**, *42*, 21443–21453. [CrossRef]
21. Bellos, E.; Tzivanidis, C.; Antonopoulos, K.A. A detailed working fluid investigation for solar parabolic trough collectors. *Appl. Therm. Eng.* **2016**, *114*, 374–386. [CrossRef]
22. Tukenmez, N.; Koc, M.; Ozturk, M. Development and performance analysis of a concentrating collector combined plant for multigeneration purposes. *Energy Convers. Manag.* **2019**, *205*, 112415. [CrossRef]

23. Kelly, N.A.; Gibson, T.L.; Ouwerkerk, D.B. Generation of high-pressure hydrogen for fuel cell electric vehicles using photovoltaic-powered water electrolysis. *Int. J. Hydrogen Energy* **2011**, *36*, 15803–15825. [CrossRef]

24. Bellos, E.; Tzivanidis, C. Enhancing the Performance of Evacuated and Non-Evacuated Parabolic Trough Collectors Using Twisted Tape Inserts, Perforated Plate Inserts and Internally Finned Absorber. *Energies* **2018**, *11*, 1129. [CrossRef]

25. Bellos, E.; Tzivanidis, C. A detailed exergetic analysis of parabolic trough collectors. *Energy Convers. Manag.* **2017**, *149*, 275–292. [CrossRef]

26. Lykas, P.; Georgousis, N.; Bellos, E.; Tzivanidis, C. Investigation and optimization of a CO_2-based polygeneration unit for supermarkets. *Appl. Energy* **2022**, *311*, 118717. [CrossRef]

27. Ahmadi, P.; Dincer, I.; Rosen, M.A. Development and assessment of an integrated biomass-based multi-generation energy system. *Energy* **2013**, *56*, 155–166. [CrossRef]

28. Ni, M.; Leung, M.K.; Leung, D.Y. Energy and exergy analysis of hydrogen production by a proton exchange membrane (PEM) electrolyzer plant. *Energy Convers. Manag.* **2008**, *49*, 2748–2756. [CrossRef]

29. Martínez-Rodríguez, A.; Abánades, A. Comparative analysis of energy and exergy performance of hydrogen production methods. *Entropy* **2020**, *22*, 1286. [CrossRef]

30. Zhang, J.; Zhang, L.; Liu, H.; Sun, A.; Liu, R.S. *Electrochemical Technologies for Energy Storage and Conversion*, 1st ed.; John Wiley & Sons: New York, NY, USA, 2012.

31. Shaygan, M.; Ehyaei, M.A.; Ahmadi, A.; Assad, M.E.H.; Silveira, J.L. Energy, exergy, advanced exergy and economic analyses of hybrid polymer electrolyte membrane (PEM) fuel cell and photovoltaic cells to produce hydrogen and electricity. *J. Clean. Prod.* **2019**, *234*, 1082–1093. [CrossRef]

32. Tzivanidis, C.; Bellos, E.; Antonopoulos, K.A. Energetic and financial investigation of a stand-alone solar-thermal Organic Rankine Cycle power plant. *Energy Convers. Manag.* **2016**, *126*, 421–433. [CrossRef]

33. Yates, J.; Daiyan, R.; Patterson, R.; Egan, R.; Amal, R.; Ho-Baille, A.; Chang, N.L. Techno-economic analysis of hydrogen electrolysis from off-grid stand-alone photovoltaics incorporating uncertainty analysis. *Cell Rep. Phys. Sci.* **2020**, *1*, 100209. [CrossRef]

34. Mehrjerdi, H.; Saboori, H.; Jadid, S. Power-to-gas utilization in optimal sizing of hybrid power, water, and hydrogen microgrids with energy and gas storage. *J. Energy Storage* **2021**, *45*, 103745. [CrossRef]

35. Lykas, P.; Bellos, E.; Caralis, G.; Tzivanidis, C. Dynamic Investigation and Optimization of a Solar-Based Unit for Power and Green Hydrogen Production: A Case Study of the Greek Island, Kythnos. *Appl. Sci.* **2022**, *12*, 11134. [CrossRef]

36. Bellos, E.; Tzivanidis, C. Concentrating Solar Collectors for a Trigeneration System—A Comparative Study. *Appl. Sci.* **2020**, *10*, 4492. [CrossRef]

37. Fouda-Onana, F.; Chandesris, M.; Médeau, V.; Chelghoum, S.; Thoby, D.; Guillet, N. Investigation on the degradation of MEAs for PEM water electrolysers part I: Effects of testing conditions on MEA performances and membrane properties. *Int. J. Hydrogen Energy* **2016**, *41*, 16627–16636. [CrossRef]

38. Papadopoulos, V.; Desmet, J.; Knockaert, J.; Develder, C. Improving the utilization factor of a PEM electrolyzer powered by a 15 MW PV park by combining wind power and battery storage—Feasibility study. *Int. J. Hydrogen Energy* **2018**, *43*, 16468–16478. [CrossRef]